Theor Chem Acc (2012) 131:1255
DOI 10.1007/s00214-012-1255-2

REGULAR ARTICLE

Stabilization of merocyanine by protonation, charge, and external electric fields and effects on the isomerization of spiropyran: a computational study

Renuka Ganesan · F. Remacle

Received: 28 February 2012 / Accepted: 3 July 2012 / Published online: 27 July 2012

Abstract Protonation, charging, and field effects on the thermal isomerization of a nitrospiropyran (SP) modified by a thiolated etheroxide chain into merocyanine (MC) are computationally studied at the DFT level. The ring opening leads to *cis*-MC conformers that then isomerize to the more stable trans forms. While the closed neutral spiropyran is more stable than the conjugated open forms, the merocyanine conformers are significantly stabilized by protonation, electron attachment, and ionization. For protonation on the pyran oxygen atom and electron attachment, the MC conformers are more stable than SP, and unlike for the neutral species, the ring opening is spontaneous at room temperature. Moreover, for the pyran oxygen-protonated form, the ring opening to the *cis*-merocyanine becomes barrierless. On the other hand, barriers comparable to the neutral remain along the thermal pathway to the *cis*-merocyanine conformer for ionization or electron attachment, and the barrier for isomerization is significantly higher for the N-protonated SP form. External field effects on the neutral reaction path show that ring opening to the *cis*-merocyanine is favored when the field reduces the electron density on the pyran part, as also induced by the local field due to O protonation.

Keywords Thermal isomerization of spiropyran · Field effects · Protonation effect · Charging effects · Quantum chemistry

1 Introduction

Spiropyran (SP) are well-known photochromes that can reversibly photoisomerize to a conjugated open form, the merocyanine (MC). The SP molecule is made of two orthogonal moieties, an indole part and a benzopyran part (see Fig. 1). The absorption of UV light causes the cleavage of the weak C4–O9 bond of the colorless closed SP form that isomerizes first to *cis*-open-MC conformers and then to more stable trans-MC ones [1–5]. All the MC conformers absorb in the visible. The conversion from a close SP form to an open planar conjugate MC form is accompanied by changes in optical, polarization, and transport properties. This reversible switching of properties upon isomerization makes spiropyran derivatives attractive candidates for designing optical switching [6–10] and storage [7, 11–13] devices, sensors [14–17] and cell imaging [18, 19].

The photochemical isomerization of various spiropyran molecules in different media (gas phase, solution, monolayers, polymers) has been extensively experimentally [1–3, 20–30] and theoretically [31, 32] studied in order to understand the reaction mechanism. Less studied, however, are the effect of protonation, charge, and external fields on the isomerization pathway of this electrocyclic reaction. It was recently reported that the rate of isomerization of the SP form is considerably increased by protonation of the

Published as part of the special collection of articles celebrating theoretical and computational chemistry in Belgium.

Electronic supplementary material The online version of this article (doi:10.1007/s00214-012-1255-2) contains supplementary material, which is available to authorized users.

R. Ganesan · F. Remacle (✉)
Department of Chemistry, B6c, University of Liège,
4000 Liège, Belgium
e-mail: fremacle@ulg.ac.be

F. Remacle
University of Liege and FNRS (Fonds National de la Recherche Scientifique), Liège, Belgium

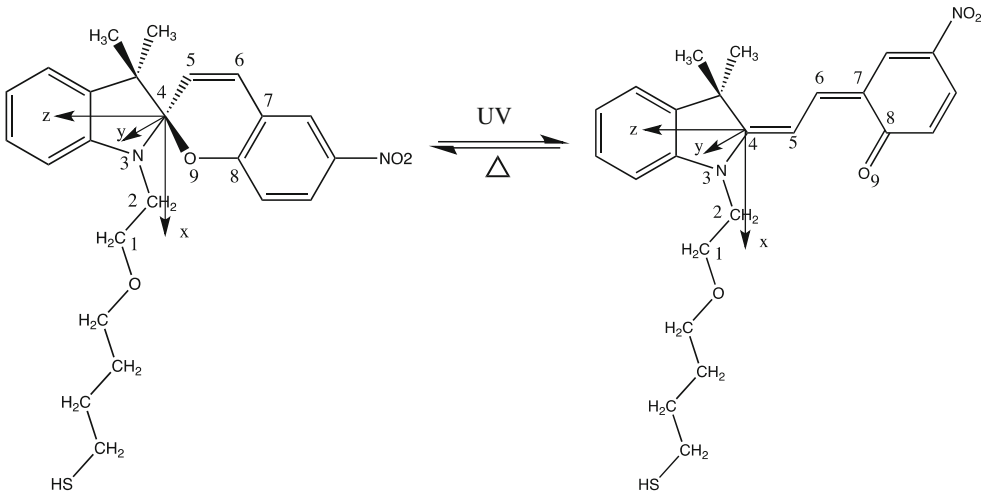

Fig. 1 Isomerization of the thiol, $(CH_2)_2O(CH_2)_4SH$, derivative of 1′,3′-dihydro-1′-R,3′,3′-dimethyl-6-nitrospiro[2H-1-benzopyran-2,2′-[2H]indole]. The carbon C4 is chiral. The spiro (SP) form is the R closed conformer (*left*) and the merocyanine (MC) the open one (*right*). The open conformers are defined by three dihedral angles α = N3–C4–C5–C6, β = C4–C5–C6–C7, γ = C5–C6–C7–C8

pyran O at room temperature [33]. This experimental finding is supported by semi-empirical computations which report that the ring opening of the O-protonated form to *cis*-MC becomes barrierless [34]. Stimulated by these results and in view of potential use of the charged and protonated forms as well as applying static fields in the design of molecular logic devices, we investigated protonation, charging, and field effects on the thermal isomerization pathway using density functional theory (DFT). For each of these effects, the Gibbs energies are calculated along the reaction coordinate. While the photoinduced SP to MC isomerization is usually faster than the thermal route, it is important to understand which processes can occur in the dark route for designing efficient and reliable devices.

Experimental photochemical studies of the neutral isomerization pathway in the gas phase [23] and in organic media [5, 35, 36] show that the ring opening of SP proceeds through several steps involving MC conformers as intermediates. They are labeled by three letters indicating a cis(C) or a trans(T) value for the α, β, γ angles defined in Fig. 1 [37]. In the first step, SP absorbs in the UV region, and the C4–O9 bond cleavage (see Fig. 1) leads to the metastable cis (CCC)-MC. The other steps are isomerizations between the different MC conformers. The most stable TTC conformer can be reached via the CCC, CTC, or TCC conformers that are metastable. The photo-activated pathways are not yet fully characterized. Uncertainties remain about the relative stability of some intermediates, like that of the CCC conformer with respect to the CTC one [38]. The reverse reaction can be induced thermally or via VIS excitation.

We focus on the 1′,3′-dihydro-1′-R,3′,3′-dimethyl-6-nitrospiro[2H-1-benzopyran-2,2′-[2H]indole] [21, 22] shown in Fig. 1 which is modified by a thiolated etheroxide chain (R = $(CH_2)_2O(CH_2)_4SH$) [13, 39–41]. Because the linker can take different conformations, there exist several stable SP conformers. In addition, the SP form has two enantiomers because the carbon atom C4 is chiral [42]. The R enantiomer is shown in Fig. 1. For each of the stable conformers of the SP form, several open MC conformers which differ by the values of three torsional dihedral angles α, β, and γ are stable. The TTC conformer is shown in Fig. 1.

We report detailed computations of the thermal reaction path and energetics of the isomerization reaction for the two enantiomers of two conformers of the SP form which differ by the value of the dihedral angle involving the linker, the C1–C2–N3–C4 dihedral angle (see Fig. 1). Our motivation for doing so is that while they are very close in energy and almost isoenergetic, the two conformers exhibit different reaction paths because of the difference of the steric hindrance due to the ligand on the ring opening. We then report on external field effects on the thermal isomerization mechanism of the neutral species. The SP form has two protonation sites: on the O atom of the pyran moiety and on the N atom of the indole part. We investigated the thermal reaction paths for both protonation sites, as well as those for the SP cation and anion.

2 Computational methodology

We use density functional theory as implemented in the suite of quantum chemistry programs Gaussian09 [43]. The choice of the functional and basis set needs to satisfy two requirements. The first one is to account correctly for the dispersion interactions that stabilize the SP form. These interactions occur between the CH_3 group on the indole part and the pyran part and induce two weak H-bonds between the H atom of the CH_3 group and the O atom of the pyran. (These bonds are indicated in Fig. 2 below). In addition to these, in the SP form, there is also a weak H-bond between a CH_2 group (H-C1 or H-C2) of the linker close to the N3 atom of the indole and the O9 atom of the

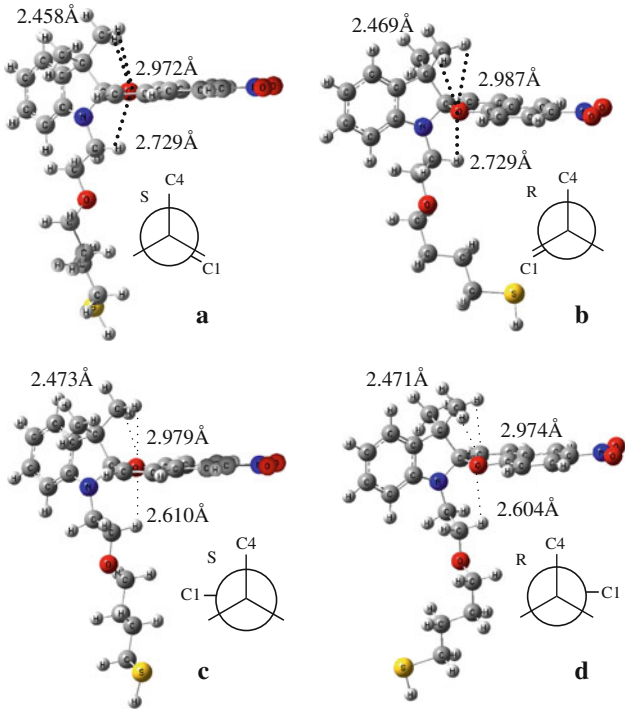

Fig. 2 Equilibrium geometries of the conformers of SP molecule shown in Fig. 1 **a** S-SP1; θ = d(C1–C2–N3–C4) = 127.2°, **b** R-SP1; $\theta = -127.6°$, **c** S-SP2; $\theta = -79.4°$, **d** R-SP2; $\theta = 79.7°$. Important H-bond between the O of the pyran and the CH_3 group of the indole and the CH_2 group of the linker, respectively, are indicated in dotted lines. For a given conformer, the two enantiomers S and R have opposite sign of the dihedral angle θ. Both enantiomers exhibit the same H-bond pattern. For S-SP2 and R-SP2, conformers with initial dihedral angle of +127° and −127° relax to stable SP2 conformers with $\theta = |79|°$

pyran (see Fig. 2 below). When the ring is opened, a stronger H-bond takes place between the O9 and the H–C5 or H–C6 group but overall the dispersions interactions are much weaker in the MC forms. The dispersions interactions occurring in the SP form make it more stable than the MC form in the neutral state which is what is observed experimentally [42]. To account for them correctly, it is necessary to use long range interaction corrected functionals [44–47]. The second effect that needs to be taken into account is the distortion of the electron density induced by applying an external static electric field. For doing so, large basis sets with diffuse functions are necessary. We use the 6-311+G(d,p) and the 6-311++G(d,p) basis sets. Two functionals were systematically investigated: B3LYP [48] and the long range interaction corrected CAM-B3LYP [45, 49]. The B3LYP/6-311++G(d,p) level accounts for the H-bond in the MC form but fails to correctly describe the long range interactions in SP and leads to numerically degenerate SP and MC conformers. On the other hand, the long range interaction corrected CAM-B3LYP/6-311+G(d,p) level leads to the experimental stability order for the neutral species, SP being more stable than MC. In addition, for this level, tests show that the energy differences between conformers, field free and in the presence of a static field do not vary when going to the larger 6-311++G(d,p) basis set (see Tables S1 and S2). We therefore report results for the CAM-B3LYP/6-311+G(d,p) level throughout the paper and when of interest, we mention results for the B3LYP functional. We also report below results obtained with the long range interaction corrected M06-2X [46] functional for the SP form which is prone to dispersion interactions.

All stable minima and TS were checked by frequency computations at the same level and the geometries of the TS confirmed by IRC computations.

3 Thermal isomerization of the neutral

Since we focus in this paper on the protonated and charged species isomerization pathways and on field effects, establishing the energetics of the thermal reaction path of the neutral thio-nitrospiropyran shown in Fig. 1 is important for comparisons at the same computational level. In addition, our study of the neutral thermal isomerization pathway provides understanding on the role of the steric hindrance and weak interactions between the linker and the SP or MC units. These effects are of interest for the isomerization of an anchored spiropyran, which is often the case for sensing, logic or storage device applications. The reason is that while the isomerization of the neutral SP to MC is usually induced by photoactivation, the MC conformers being less stable than the SP form, the back isomerization can occur thermally. The characterization of the isomerization barriers between the different merocyanine conformers is also of interest as the final steps of the forward photochemical pathways.

We first investigated the relative stabilities of the different conformers. Those are mainly of the MC form. However, the SP form has two enantiomers because it has a chiral center, C4 in Fig. 1. In addition, several almost isoenergetic conformers of the SP and the MC are possible because of the different conformations of the linker chain. Among those, we investigated in details two conformers of the SP form that differ by the value of the dihedral angle d(C1–C2–N3–C4) (see Fig. 1). These two conformers have a different pathway for the opening of the cycle due to differences in the steric hindrance of the linker. Since each of them has two isoenergetic enantiomers, we report on the isomerization pathways of four SP conformers. Their computed equilibrium geometries are shown in Fig. 2, and the energetics and some relevant geometry parameters of each conformers are reported in Table 1. The pair of enantiomers that we call SP1 is the lowest in energy when

Table 1 Relative ZPE corrected and free energies (kJ mol^{-1}) of the SP and MC conformers as well as of the transition states along the isomerization pathways reported in Fig. 3, computed at CAM-B3LYP/6-311+G(d,p) level (with respect to S-SP1)

Conformer	$\Delta E\ ZPE_{corrected}$	ΔG	C4–O9	θ	α	β	γ
S-SP1	0.0	0.0	1.467	127.2	124.9	−1.5	−2.2
S-SP2	1.3	4.2	1.474	−79.4	131.8	−2.5	−4.9
R-SP1	0.5	2.8	1.466	−127.6	−128.3	1.9	3.8
R-SP2	1.3	4.9	1.474	79.7	−131.3	2.4	4.7
TTCa	40.3	35.8	4.133	85.7	178.2	178.4	−1.4
TTTa	45.3	42.5	4.977	95.4	178.0	179.0	179.9
CTCa	47.4	50.9	4.148	86.9	−8.9	178.8	−0.9
CTTa	51.0	48.3	5.019	94.3	−11.7	−178.3	174.2
S-CCCa	68.1	68.4	2.637	95.4	42.5	16.7	14.1
CCTa	85.2	78.1	5.275	84.0	22.7	26.0	−176.7
TCTa	115.9	113.0	5.339	87.6	179.7	−3.0	178.7
TTCb	41.7	38.5	4.128	−84.7	−178.3	−177.8	1.8
TTTb	47.9	44.6	4.970	−98.2	−178.6	−178.3	−179.7
CTCb	53.2	51.2	4.115	−94.5	10.8	178.6	2.7
CTTb	51.0	51.5	5.026	−93.9	11.4	178.6	−174.4
R-CCCb	70.1	68.7	2.636	−98.2	−42.8	−16.6	−13.4
CCTb	94.9	98.0	5.292	−123.3	17.6	35.6	−175.7
TCTb	116.8	112.2	5.339	−87.8	179.8	3.9	−178.4
TS1	68.8	73.0	2.361	101.9	62.1	11.6	14.9
TS2	125.4	118.3	3.354	89.6	−3.6	94.4	−4.9
TS3	115.2	113.3	4.042	88.9	90.9	−178.8	1.7
TS4	125.2	121.4	3.342	90.0	179.2	−88.5	−0.1
TS5	70.8	74.5	2.374	−104.6	−61.5	−11.8	−14.5
TS6	117.9	123.3	3.389	−91.8	5.9	−96.0	4.7
TS7	118.0	116.9	4.038	−88.0	−91.1	179.4	−1.9
TS8	125.3	121.3	3.339	−90.2	−179.2	88.7	−0.1
TS9	123.6	128.0	3.413	−95.6	−4.0	98.8	−6.0
TS10	122.3	119.2	3.327	−79.2	179.2	−87.0	−1.4
TS11	123.3	119.2	3.359	96.6	−0.2	−94.4	2.9
TS12	122.2	118.3	3.330	79.5	−179.3	87.1	1.4

The corresponding values of the C4–O9 bond (in Å) and dihedral angles θ = d(C1–C2–C3–N4), α = N3–C4–C5–C6, β = C4–C5–C6–C7, γ = C5–C6–C7–C8 (in degree) (see Fig. 1) are also reported. The difference between the $\Delta E\ ZPE_{corrected}$ and ΔG for S-SP1 is −173.8 kJ mol^{-1}

computed at the CAM-B3LYP/6-311+G(d,p). They correspond to a value of the dihedral angle d(C1–C2–N3–C4) of |127|°. The second pair of stable enantiomers exhibits a value of the dihedral angle d(C1–C2–N3–C4) of |79|° and is called SP2. The SP2 enantiomers are also isoenergetic within numerical accuracy, see Table 1. On the other hand, the SP1 and SP2 conformers differ by the trans (SP1)- or the cis (SP2)-orientation of the C1–C2 bond of the linker with respect to the C4–O9 bond of the pyran. This difference leads to more steric hindrance for the opening of the C4–O9 bond for the SP2 conformers and to higher energy barriers as discussed below. It also plays a role in N-protonated isomerization pathway (see Sect. 5).

The order of stability of the SP1 and SP2 conformers depends on the relative strength of the two kinds of H-bonds that can take place : those between the CH_3 group of the indole and O of the pyran and the H-bond between one of the CH_2 group of the linker and the O of pyran, see Fig. 2. In the S-SP2 conformer, the H-bond takes place between the C1 carbon of the linker and the O of the pyran part, while for the S-SP1, it is the C2 carbon of the linker that is involved. The SP1 and SP2 conformers are computed to be numerically quasi degenerate. The energy difference between them being small, their order of stability depends on the functional used. At the CAM-B3LYP/6-311+G(d,p) level, the linker-pyran H-bond is stronger in SP2 and leads to a more rigid geometry for SP2 with systematically slightly larger vibrational frequencies for the lowest normal modes (see Fig. 2). The computed free energy difference at 298 K between the S-SP1 and S-SP2

conformers is 4.2 kJ/mol. This energy difference is mainly due to the entropy effect, the zero point energy (ZPE) corrected energy difference between two conformers being 1.3 kJ/mol, see Table 1. The same is true at the B3LYP/6-311+G(d,p) level, see Table S3. On the other hand, at the M06-2X/6-311+G(d,p) level, both kinds of H-bond are stronger in SP2 than in SP1, which leads to a reverse of the order of stability with respect to the CAM-B3LYP level, SP2 being more stable than SP1 by 1.7 kJ/mol for electronic energies, see Table S3.

The two enantiomers of a given conformer follow the same reaction pathway. However, the opening of the C4–O9 bond in the R and S enantiomers of SP1 and SP2 does not lead to the same family of MC conformers, again because of a different orientation of the linker. S-SP1 and R-SP2 lead to positive values of the dihedral angle θ ranging between $+84.0°$ and $+95.4°$ in the planar MC conformers (labeled MCa), while for R-SP1 and S-SP2, the values of the dihedral angle θ are negative and range between $-84.7°$ and $-123.3°$ (labeled MCb) (see Table 1). The energies and geometries are reported in Table 1 and in Fig. S1 of the ESM. Each conformer of MCa is quasi isoenergetic with the corresponding MCb one with free energy differences in the range 0.5–3.0 kJ/mol except the CCT conformer for which the computed energy difference between CCTa and CCTb is 19.9 kJ/mol. Note that this conformer is not involved in the reactions we discussed below. Barriers for isomerization among the MCa or the MCb conformers are in the range of 50–70 kJ mol^{-1}, see Table 1 and Fig. 3. The stability order of MCa open conformers at the CAM-B3LYP/6-311+G(d,p) level is computed to be:

$$\text{TTCa} > \text{TTTa} > \text{CTTa} > \text{CTCa} > \text{CCCa} > \text{CCTa} > \text{TCTa} \quad (1)$$

while for the MCb conformers, we get:

$$\text{TTCb} > \text{TTTb} > \text{CTCb} > \text{CTTb} > \text{CCCb} > \text{CCTb} > \text{TCTb} \quad (2)$$

The TCC conformer is not stable because of the steric hindrance due to the methyl group and relaxes to the SP conformer upon geometry optimization. A trans configuration for the dihedral angle β has less steric hindrance. In agreement with ref [50], conformers that are trans (T) for the β dihedral angle (TTC, TTT, CTC, CTT) are therefore computed to be more stable than conformers that are cis for that angle (CCC, CCT, TCT). TTC and TTT are found to be more stable than other MC conformers in agreement with refs [21, 51, 52]. In the gas phase, SP is more stable than TTC. The zero point energy (ZPE) corrected energy difference between the S-SP1 and TTCa is 40.3 kJ/mol at the CAM-B3LYP/6-311+G(d,p) level and the free energy difference is 35.8 kJ/mol at 298 K, see Table 1. (Using the B3LYP functional without long range corrections, SP and TTC are closer in energy, ΔG is 14.5 kJ/mol at B3LYP/6-31G(d,p) and 1.2 kJ/mol at B3LYP/6-311 ++G(d,p), see Table S1. The larger stability of the SP form implies that the thermal back isomerization to SP is spontaneous at room temperature, in agreement with experimental results [42]. On the other hand, as we report below, charging or protonation of the SP stabilizes the MC forms compared to the SP one. In the case of the anion and the O-protonated species, the order of stability is reverted and MC is more stable than SP, making the forward reaction (ring opening) spontaneous at room temperature.

The neutral isomerization pathways for the SP1 and the SP2 conformers were first screened using a grid in the α and β dihedral angles while keeping all other coordinates frozen. Since varying these angles de facto implies a variation of the CO bond length, the identified stable points (maxima and minima) were then relaxed and the transition state geometries confirmed by IRC. All the maxima and minima are checked by frequency calculation. The two pathways important for the thermal isomerization and for comparison with the charged species are reported in Fig. 3 for each enantiomer of the SP1 and SP2 conformers. For a given conformer, the reaction pathways of the two enantiomers are identical within numerical accuracy.

The reaction pathway for the SP1 conformer (Fig. 3a, b) involves as a first intermediate the metastable CCC MC conformer, which can easily revert to the SP form. The computed barrier at room temperature from S-SP1 to CCCa is 73.0 kJ/mol (Fig. 3a), while the reverse barrier is only 4.6 kJ/mol. The computed transition state theory (TST) forward rate constant is 9.7×10^{-1} s^{-1}, while the backward rate is 9.7×10^{11} s^{-1}. For this reason, the CCC conformer has not been unambiguously identified experimentally [38]. Its geometry is distorted and not fully planar, unlike that of the more stable MC conformers. To reach the more stable CTCa and TTCa MC open conformers, one needs to cross two other high barriers (49.9 kJ/mol and 62.4, respectively). For these two final steps, the forward reaction is faster than the backward one. The TST forward and backward rates between each intermediate are reported in Table S4. Since the neutral TTC and CTC forms are higher in energy than the SP1 closed conformer, at room temperature, it is the colorless SP1 form that is by far preponderant. We also report in Fig. 3a and b a second reaction pathway, which goes directly via a single TS from the S-SP1 to the TTCa form with a barrier 121.4 kJ/mol. This pathway will be shown to be of interest for comparison with the pathways of the charged species.

As alluded to above, for the SP2 conformer (see Fig. 2c, d), the reaction path is different because of the steric hindrance of the (thiol derivative) linker: at the equilibrium geometry,

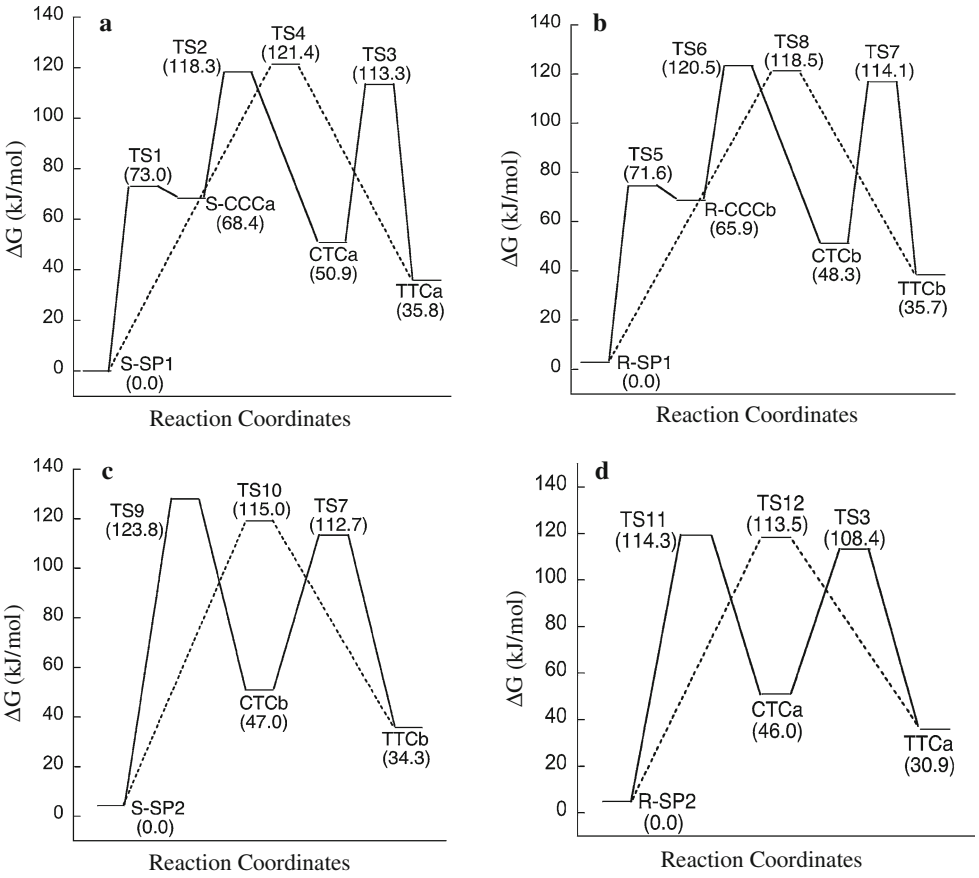

Fig. 3 The two investigated thermal reaction pathways of the isomerization reaction of S-SP1 (**a**), R-SP1 (**b**), S-SP2 (**c**), R-SP2 (**d**) to MC. The free energies are calculated at the CAM-B3LYP/6-311+G(d,p) level in the gas phase at room temperature and reported with respect to the S-SP1 conformer in all four panels. Energy differences in parenthesis are computed with respect to corresponding stable SP conformer for each panel. The multistep reaction path is shown in solid line and the direct one in dotted ones. See also Table 1

the linker is positioned in the ring opening direction. For this reason, the CCC conformer is not stable for the SP2 form. SP2 is isomerizing directly to CTC via a very high barrier of 123.8 kJ/mol (Fig. 3c). CTC is not chiral anymore and can isomerize to TTC as in Fig. 3a and b. On the other hand, the direct one step isomerization from SP2 to TTC has a barrier of 115.0 kJ/mol at CAM-B3LYP/6-311+G(d,p) level (see Table 1). This energy barrier is slightly lower than that of the isomerization of the SP1 conformer discussed above.

4 Field effects on the neutral reaction pathway

We first report on the effect of a static external field on the electrocyclic reaction leading to ring opening. The effect of the static field is to distort the electronic density and to change the distribution of partial charges. Our motivation is to investigate whether reasonable field strength of about 1 V/nm, as typically applied in break junctions, could distort the electron density strongly enough to induce the ring opening of the SP form. Significant field effects have been recently reported by Shaik et al. [53] on another electrocyclic reaction, the one step Diels-Adler reactions between butadiene and ethylene and between maleic anhydride and cyclopentadiene. The situation is more complex in the case of the isomerization of the SP because the most favorable reaction path is multistep and involves several intermediates. Our conclusion is that while the electronic density is significantly distorted, as shown in Fig. 4 below, reasonable field strength cannot lead to a ring opening.

We started by systematically analyzing the changes in the distribution of the electron density between the two moieties for increasing field strengths of different orientations with respect to the molecular frame shown in Fig. 1 for the neutral S-SP1 conformer (see Fig. 2a) at its field-free equilibrium geometry. As pointed out in Ref. [53], in Gaussian09, the direction of the applied external field corresponds to the displacement of negative charges. Since the reaction coordinate for the opening of the C4–O9 bond has components in the y and z directions, we concentrated on these two directions. The field effects along the x direction mainly affect the linker part. The effects on the relative energies of the TS and the metastable intermediates for field strengths of 1.3 V/nm applied the x, y, and z directions (see Fig. 1) are reported in Table S5. We show in Fig. 4 the difference, $\rho_{F=0} - \rho_{F_z}$, between the field-free and field-distorted isocontours of the one-electron density of SP for a field strength of 1.3 V/nm applied in the

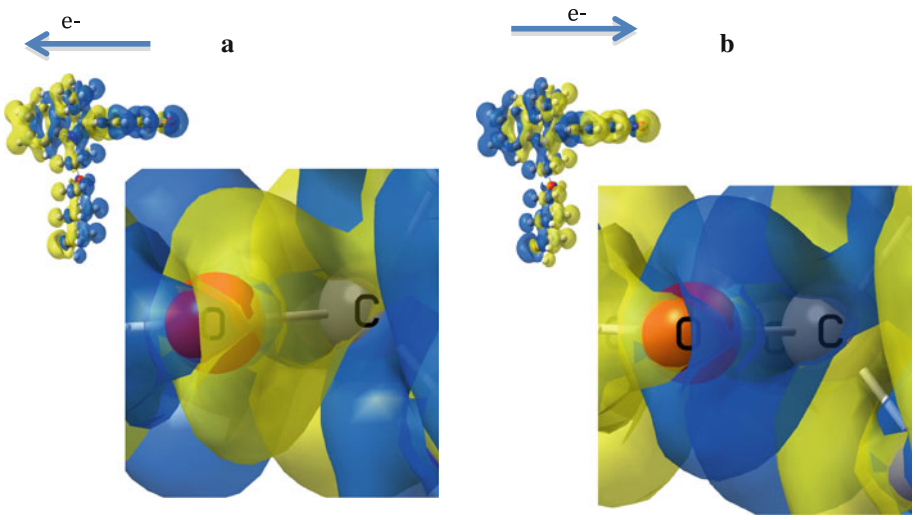

Fig. 4 Zoom on the C4–O9 bond of an isocontour of the density difference, $\rho_{F=0} - \rho_{F_z}$, where $\rho_{F=0}$ is field free and ρ_{F_z} is computed for an external field strength of 1.3 V/nm applied in z direction (*panel a*) and $-z$ direction (*panel b*) at the CAM-B3LYP/6-311+G(d,p) level for the equilibrium geometry of the field free S-SP1 molecule. Isocontour value is 0.0001 |el/Å^3. The insets show the overall molecule oriented as in Fig. 1. A positive difference is shown in *blue* and a negative one in *yellow*. A negative difference (*yellow*, *panel a*) indicates that the finite field electron density is larger than that of the neutral. A positive difference (*blue*, *panel b*) indicates that the electron density of the neutral is larger than that of the field distorted one so that the field has decreased the density on the C4–O9 bond. Accordingly, the z component of the dipole moment computed for a field applied in the $+z$ direction is 0.3 D which is smaller than that of the neutral (2.8 D), while the dipole moment computed for a field applied in the $-z$ direction is +5.3 D, which is larger than that of the neutral. See Fig. S2 for the difference between the field free and the field distorted isocontours of the one-electron density of the TTCa open form

$+z$ (Fig. 4a) and $-z$ (Fig. 4b) directions (see Fig. 1). The figures show specifically the C4–O9 bond and the insets the entire molecule. As a general rule, an orientation of the external field that favors a decrease of electron density on the pyran moiety, in particular on the C4–O9 bond, favors ring opening. This corresponds to the $-z$ direction and $-y$ directions for which the electron density increases on the nitrobenzene part moiety and decreases on the indoline part and on the C4–O9 bond of the pyran (see Fig. 4b).

We then optimized the geometries of the intermediates reported in Fig. 3 and in Table 1 for a field strength of 0.0025 a.u. (corresponding to 1.3 V/nm) applied in the $+z$, $-z$, $+y$, and $-y$ directions. The results are reported in Table 2. Partial charges were computed for the field-free and the finite-field equilibrium geometries. The changes in partial charges while small at this field strength reflect the changes induced in the localization of the electron density of the applied external field shown in Fig. 4 and are reported in Table S6 of the ESM. The changes in partial charges are larger when computed using the MK [54] approach than using the NBO [55] one. The MK partial charges increase significantly on the C4 (positive, 20–40 %) and O9 (negative, a few %) atoms for field applied in the $+y$ and $+z$ direction. They decrease but to a smaller extent when the field is applied in the $-y$ and $-z$ directions. The NBO analysis [55] gives smaller partial charge changes. This analysis also gives a small increase of electron density on the C4–O9 bond when the field is applied in the $+y$ and $+z$ directions and a decrease for field applied in the opposite directions. The changes in the equilibrium geometry C4–O9 bond length induced by the external field are consistent with the changes in the localization of the electron density and in the computed partial charges reported above. The C4–O9 bond length increases by 0.01 Å for a field strength of 0.0025 a.u. applied in the $-y$ and $-z$ direction which favors the bond opening. For a stronger field of 0.005 au (2.6 V/nm), the C4–O9 bond length increased is of about 0.03 Å at the B3LYP/6-311 ++G(d,p) level.

A field applied in the $-y$ and $-z$ directions lowers the barrier for the ring opening step, between S-SP1 and S-CCCa, from 73.0 kJ/mol (field free) to 61.9 kJ/mol for a field applied in the $-y$ and 60.2 kJ/mol for a field applied in the $-z$ direction (Table 2). A similar trend in the lowering of the barrier is induced by the effect of a nitro group in para to C4–O9 bond in spiropyran. The nitro group, being an electron attractor, also depletes the electron density on the C4–O9 bond [31]. When the static field is applied in the $+y$ direction, the trans-MC CTCa and TTCa conformers are less stable than SP by 42.5 and 20.8 kJ/mol, respectively, while when the field applied in the $-z$ direction, the CTCa and TTCa conformers are less stable than S-SP1 by 27.2 and 16.4 kJ/mol but more stable than in the field-free case (see Table 2). On the other hand, a field

Table 2 Relative free energies (kJ mol^{-1}) for the two reaction pathways of the neutral molecule (see Fig. 3) computed at CAM-B3LYP/6-311+G(d,p) level for an external electric field of 1.3 V/nm applied in the y and z directions (see Fig. 1)

Conformer	Field free	y	$-y$	z	$-z$
S-SP1	0.0	13.0	−16.1	5.9	−10.7
CCCa	68.4	83.7	39.7	79.1	45.6
CTCa	48.3	55.5	44.7	68.7	16.5
TTCa	35.8	33.8	30.5	52.8	5.7
TS1	73.0	88.7	45.8	84.8	49.5
TS2	118.3	124.6	109.6	120.6	105.7
TS3	113.3	118.1	97.5	150.4	64.4
TS4	121.4	126.6	110.5	121.7	111.1

The relative energies of the conformers and TS at finite field are reported with respect to field free S-SP1 conformer. All computed frequencies of the stable conformers are real, and the TS have a single imaginary frequency only

applied in the $-z$ direction does not favor the isomerization from CCC to CTC. Overall, it is therefore not possible to find a single field orientation that leads to a significantly faster isomerization rate from SP to TTC. If, however, one is interested in controlling one isomerization step along the reaction pathway, like for example as recently reported for the TTC and the TTT MC conformers, [52] field effects can be significant. Since SP and MC have rather large dipole moments, the computed values at the CAM-B3LYP/6-311+G(d,p) are 9.8 D for TTC compared to 6.4 D for SP, the molecules could be oriented and the switching between two forms controlled by applying a static electric field.

5 O and N protonation effects

Compared to applying a static external field, fully charging the molecule, either by removing or adding an electron or by adding a proton, significantly modifies the relative stability of the close and open conformers and the reaction pathways.

A recent experimental study on protonation effect [56] as well as previous studies [33, 34] shows that protonation on the pyran oxygen considerably stabilizes the open form, see Fig. 5. These studies report that the colorless SP opens to *cis*-MC by protonation of the pyran oxygen at room temperature. Isomerization to the most stable MC TTC conformers can be induced by UV light. The reverse reaction can be triggered by moving to a basic solution or by VIS light. Protonation on the N atom of the indole cycle was also observed as a side product [33].

Our computations fully confirm this effect. Protonation on the O of the pyran significantly decreases the electron density on the C4–O9 bond, which leads to the opening of the bond. Upon O protonation, both enantiomers of the SP1 and SP2 forms are found unstable. They relax to the open *cis*-$TCCOH^+$ conformer (as shown in Fig. 6, see also Table S7) that was not identified in the neutral reaction pathway. On the other hand, protonating the SP form on the N atom accumulates electron density on the C4–O9 and the indoline part, which stabilizes significantly the SP forms, see Fig. 6 and Table S8. The effects of O and N protonation are similar to those reported above for externally applied electric fields. The difference is that the local field created by protonation is stronger than those induced by a reasonable field strength. Protonation on the O of the pyran is strong enough to lead to the opening of the C4–O9 bond, while reasonable field strengths (< than 2.6 V/nm) remove electron density from that bond (Fig. 4b) and accumulate electron density on the nitrobenzene part but do not trigger bond opening. N protonation accumulates electron density of the C4–O9 bond and leads to a larger stabilization of the SP form than external fields applied in the $+z$ and $+y$ directions. The analog of Fig. 4 computed for protonation effects on the one electron density difference is reported in the ESM, Fig. S3.

The computed reaction pathways for the O-protonated SP are reported in Fig. 7 (see also Table S7) for the two enantiomers of the SP1 and SP2 conformers. Upon geometry optimization, $SPOH^+$ is not stable and relaxes to the stable $TCCOH^+$. The $CCCOH^+$ conformer is found slightly more stable than the $TCCOH^+$ conformers (by 3–7 kJ mol^{-1}) except for R-SP2 where it is $TCCOH^+$ which is more stable by 18.7 kJ mol^{-1}. The *cis*-$MCOH^+$ conformers then isomerize to trans-$MCOH^+$.

As in the case of the neutral (see Fig. 3), the protonated S-SP1 and R-SP2 go to protonated MCa conformers, while R-SP1 and S-SP2 lead to MCb conformers. The $CCCOH^+$ and $TCCOH^+$ conformers do not isomerize easily to the stable trans-O-protonated MC form. The computed barriers for the isomerization of $CCCOH^+$ to $CTCOH^+$ are of the order of 120 kJ mol^{-1}. The second isomerization between $CTCOH^+$ and $TTCOH^+$ is easier, with computed barriers of the order 20 kJ mol^{-1}.

For the N-protonated SP, there are two possible ways for the proton to bind to the N atom (see Fig. S4). This in total

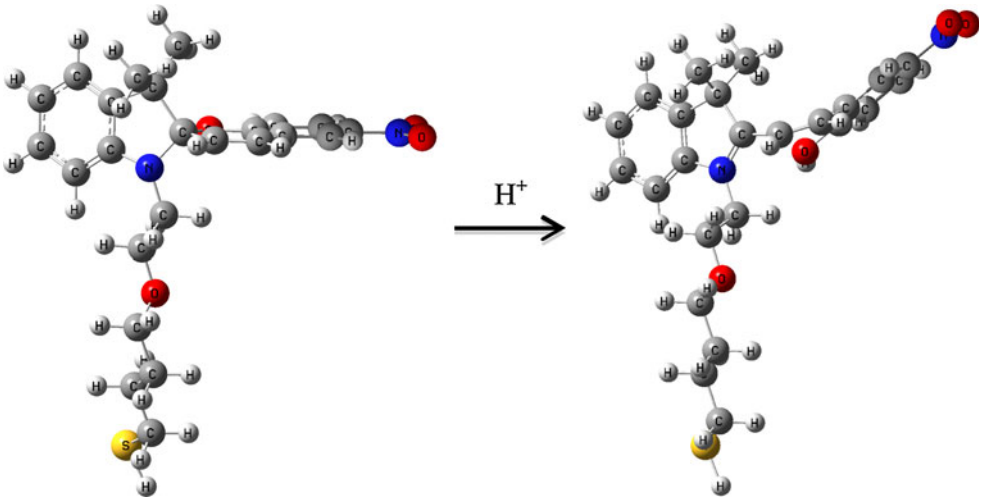

Fig. 5 S-SP1(left) and protonated open stable $TCCOHa^+$ (*right*) calculated at CAM-B3LYP/6-311+G(d,p). Note that the SP-O-protonated form is not stable

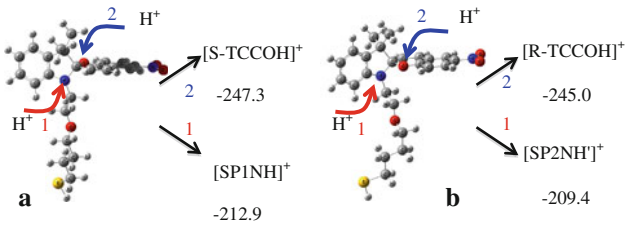

Fig. 6 **a** Protonation on O and on N of S-SP1 conformer, **b** protonation on O and on N of R-SP2 conformer, as for the neutral case, both enantiomers of a given conformer react in the same way (see Fig. 7). The protonation free energies (kJ mol^{-1}) for the reaction SP + $H_3O^+ -> SPH^+ + H_2O$ are computed at the CAM-B3LYP/6-311 + G(d,p) level at room temperature. Note that while protonation on the O leads to the open *cis*-$TCCOH^+$ conformer (see Table S7), protonation on the N atom leads to a stable close SP conformer (see Table S8)

leads to eight possible conformers of the N-protonated form. When the N–H bond is in a trans configuration with respect to the C4–O9 bond of the benzopyran, the conformer is named as $SPNH^+$, while it is called $SPNH'^+$ when the N–H bond is cis with respect to the C4–O9 bond. The enantiomers of $SP1NH^+$ are more stable than the $SP1NH'^+$ ones by about 13.3 kJ/mol. On the other hand, the R and S enantiomers of $SP2NH^+$ and $SP2NH'^+$ are found to be isoenergetic. In the case of N protonation, the close conformers are considerably more stable than the open ones (by about 100 kJ/mol). No stable $CCCNH^+$ conformer could be identified in the reaction pathways. Upon ring opening, the SP1 enantiomers go to $CTCNH^+$ conformer with very high barriers of 190 kJ/mol (see Table S8).

To summarize, for all conformers of SP, the protonation of the O of the pyran leads to a localization of positive charge on the benzopyran part, which favors the opening of the C–O bond and the conversion to a distorted $TCCOH^+$ conformer without any barrier. On the contrary, the N-protonated form is very stable for all SP conformers and compared to the neutral case significantly more stable than the open MC conformers.

6 Electron attachment and ionization effects

Experimental studies of the electrochemical oxidation and reduction of nitro SP compounds in different environments show that oxidation takes place on the indole part of the SP and reduction at the NO_2 group of the benzopyran part of the SP [57–60]. Without a NO_2 group, SP does not exhibit electroactivity [61]. We report in this section on the isomerization reaction pathways for the anion and the cation of S-SP1 conformer. The isomerization pathways are summarized in Fig. 8 and compared with field and protonation effects.

The vertical attachment of an electron to the neutral S-SP1 form leads to a localization of the extra electron density on the benzopyran part mainly on the NO_2 group. This density corresponds to that of the LUMO of the neutral, see Fig. 9a. Since the ring opening and the breaking of the C4–O9 bond is favored by a decrease of electron density on the benzopyran part, the computed barrier for ring opening remains high, similar to neutral one, and is equal to 85.9 kJ/mol (see Fig. 8a, f). The difference is that the $CCCa^-$ anion is more stable than the $S\text{-}SP1^-$ anion by 8.6 kJ/mol, so that the back reaction is not spontaneous, unlike what is found for the neutral. Being stable, it is also likely that the $CCCa^-$ conformer could be easily identified spectroscopically. The $CTCa^-$ and $TTCa^-$ anions are also more stable than $S\text{-}SP1^-$ by 43.9 and 59.0 kJ/mol, respectively, (see Fig. 8f and Table S9) and the forward isomerization barrier of the $CCCa^-$ conformer to the more stable open $CTCa^-$conformer is computed to be 16.6 kJ/mol, which leads to a very fast isomerization rate of 7.9×10^9 s^{-1}. The computed TST

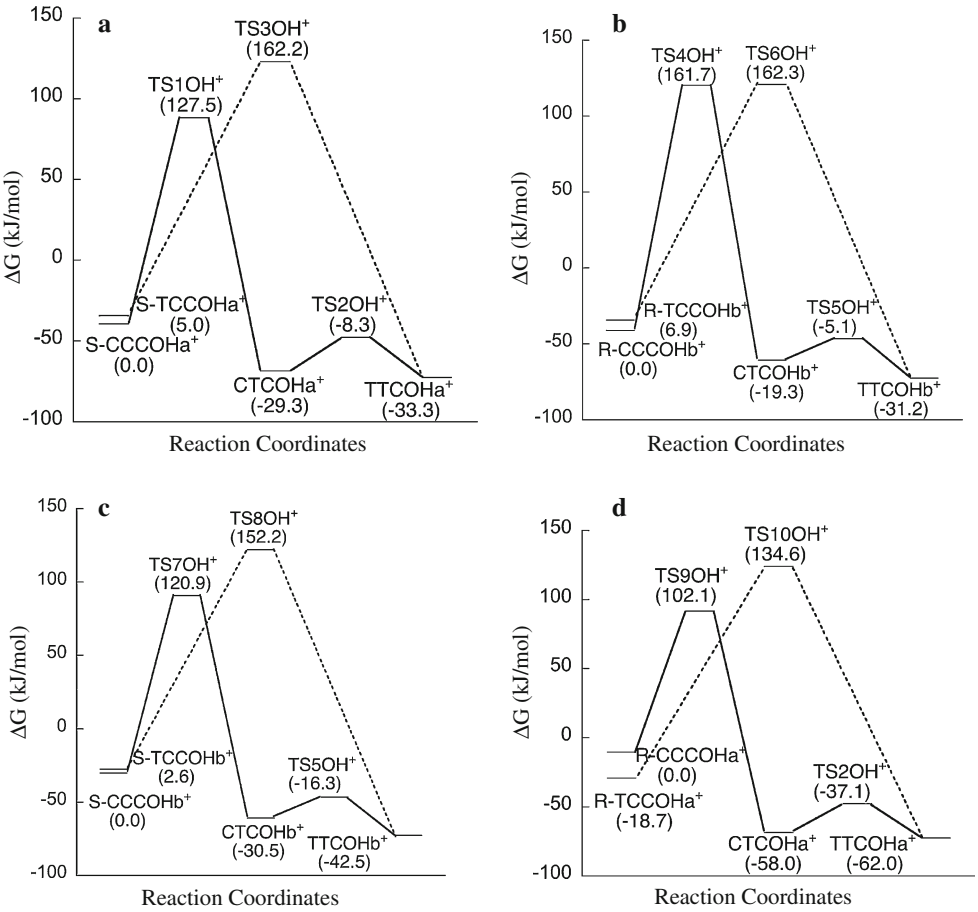

Fig. 7 **a** Free energy profile for the protonated SP: **a** S-SP1, **b** R-SP1, **c** S-SP2, **d** R-SP2 computed with respect to the stable N-protonated S-SP1 conformer. Energies in parenthesis are computed with respect to the stable corresponding $CCCOH^+$. The free energies are calculated at CAM-B3LYP/6-311+G(d,p) level in the gas phase at room temperature. See also Table S7

rates are reported in Table S10. In the case of the anion, we also identified a different reaction path involving the $TCCa^-$ conformer. This reaction pathway involves fewer intermediates and does not exist for the neutral. The $CCCa^-$ conformer can isomerize to the $TCCa^-$ intermediate by crossing a barrier of 42.1 kJ/mol. One can then reach $TTCa^-$ in an essentially barrierless manner (the computed barrier is 4.7 kJ/mol). Since the anion forms of MCs are stabilized compared to the SP anion, the backward reaction is not spontaneous but can be induced by VIS light. However, unlike in the case of protonation on the O of the pyran (see Fig. 8b), the ring opening to $CCCa^-$ is not spontaneous, the computed rate constant is 5.4×10^{-3} s^{-1} (see Table S10), the thermal reaction is slow but occurs spontaneously. The next reaction steps involving isomerization between the MC forms are much faster.

Upon vertical ionization, a hole is made in the indoline part, which leads to a decrease of the electron density and partial charge on the N atom. The hole density corresponds to the density of the HOMO of the neutral, see Fig. 9b. Upon geometry relaxation, the geometry of the S-SP1 cation is distorted with respect to that of the neutral (in particular the α dihedral angle) but remains more stable than that of the open $CCCa^+$ MC conformer by 28.8 kJ/mol (see Fig. 8e and Table S11). The energy difference is smaller than in the case of the neutral (see Fig. 8a) and the barrier height for the isomerization to $CCCa^+$ is computed equal to 73.6 kJ/mol. $S\text{-}SP1^+$ remains more stable than $TTCa^+$ by 8.3 kJ/mol while for the neutral S-SP1 is more stable than TTCa by 35.8 kJ/mol. The energy barrier for the isomerization of CCCa to TTCa is 60.4 kJ/mol, the TS of this isomerization step being similar to the TS4 of the neutral. Unlike for the reaction paths of the neutral (Figs. 3, 8a) and of the anion (Fig. 8f), the reaction path of the cation involves only two intermediates. The computed rates of isomerization can be found in the Table S12. Contrary to electron attachment, the isomerization of the SP cation is not spontaneous at room temperature. The isomerization pathway is similar to that of the neutral.

7 Concluding remarks

Protonation, charge, and field effects affect the thermal reaction path of the isomerization of spiropyran. Since these effects are likely to occur when the isomerization takes place in solution or in a break junction, it is of interest to characterize them in order to design reliable sensing,

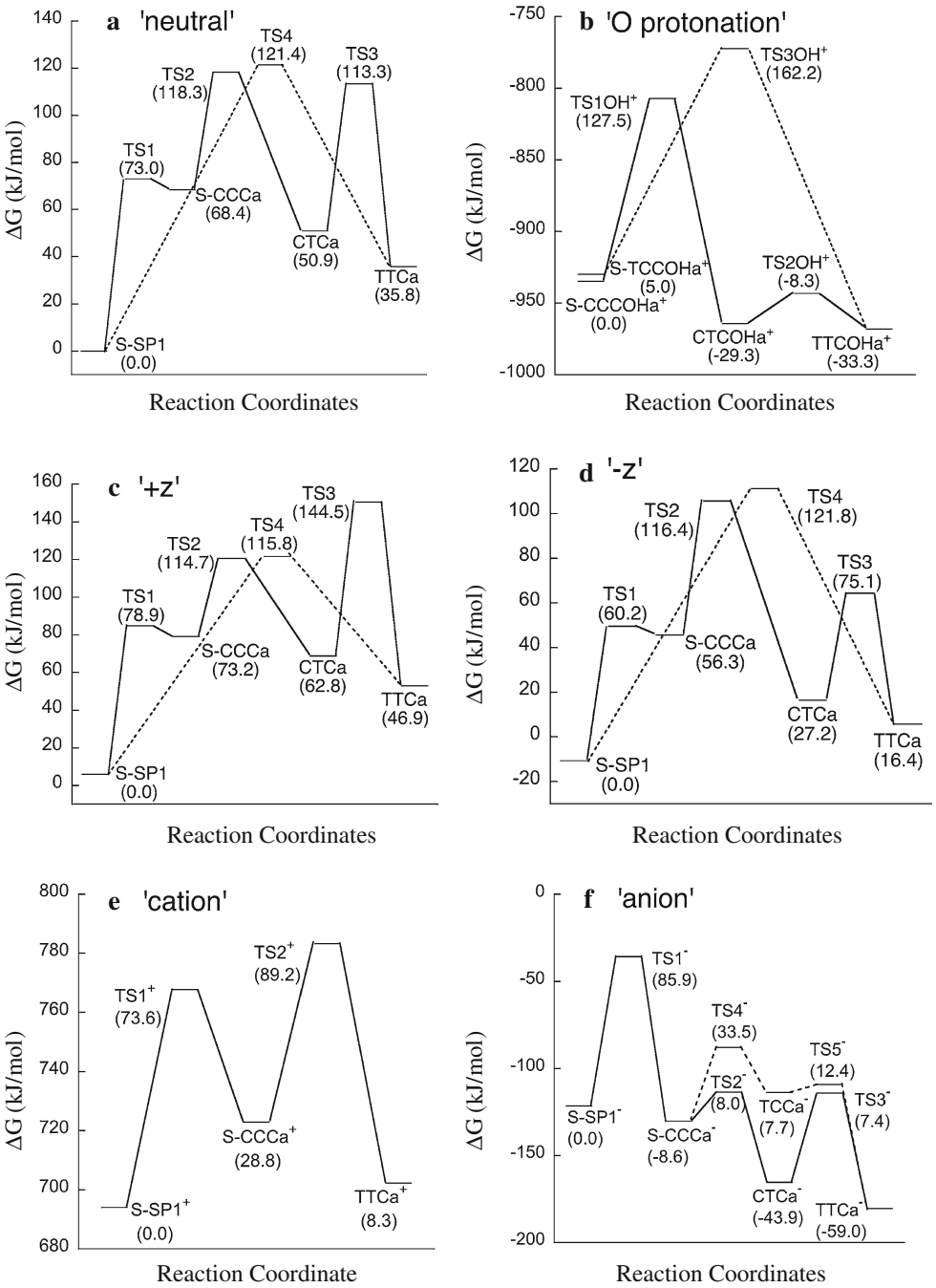

Fig. 8 The thermal reaction pathways of the isomerization reaction of S-SP1 to MCa under different conditions: **a** neutral, **b** proton attachment **c** field (1.3 V/nm) applied in the z direction, **d** field (1.3 V/nm) applied in the $-z$ direction **e** removing an electron **f** adding an electron. The free energies are calculated at the CAM-B3LYP/6-311+G(d,p) level in the gas phase at room temperature and reported with respect to neutral S-SP1. Energy differences in parenthesis are computed with respect to corresponding SP conformer for **a**, **c**–**f**, in **b** computed with respect to S-CCCOHa$^+$ conformer

logic, or storage devices. Our computational results are summarized in Fig. 8 above. They show that charge effects stabilize the open MC conformers with respect to the close SP form and reverse the order of stability in the case of electron attachment (Fig. 8f) and protonation on the O of the pyran (Fig. 8b), so that the ring opening becomes spontaneous at room temperature. While a marked increase of the rate for ring opening was experimentally reported for the oxygen-protonated form, [33] the cation and the anion reaction pathways have not yet been experimentally investigated. The largest effect on the reaction pathway occurs in the case of protonation on the O of the pyran moiety for which we could not identify a stable SP form. Upon relaxation, the stable conformer is an open *cis*-MCOH$^+$ conformer. The latter then isomerizes to the trans-MC form. For the anion (Fig. 8f), the CCC form is more stable than the SP one, as well as all the trans-MC conformers. In the case of the cation (Fig. 8e), the CCC and TTC conformers remain less stable than SP. While the ring opening is barrierless for protonation on the O of the pyran

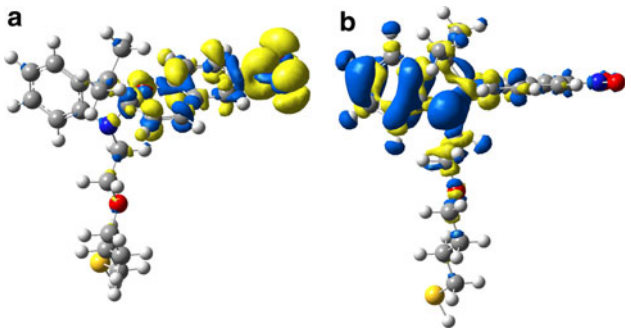

Fig. 9 Isocontour (0.002 |e|/Å^3) of the density difference between the neutral S-SP1 and the S-SP1 anion, $\rho_{SP} - \rho_{SP-}$, (**a**) and the S-SP1 cation, $\rho_{SP} - \rho_{SP+}$ (**b**) computed at the CAM-B3LYP/6-311 + G(d,p) level. In (**a**), the geometry is rotated by 30° with respect to S-SP1 (see Fig. 2). One can see that the extra electron density is localized on the benzopyran part and particularly on the nitro group. On the other hand, the hole is localized on the indoline part (**b**)

moiety, for the anion and the cation, the computed rates are of the same order of magnitude as those computed for the neutral. The N-protonated SP form is found very stable.

As a general rule, the electrocyclic reaction leading to ring opening is favored when the electron density of the pyran part is reduced. The decrease of the electron density on the C4–O9 bond leads to the stable TCC form in the case of protonation on O9 (Fig. 8b) and to a decrease of the barrier height to reach CCC upon application of an external electric field that withdraw electron density from that bond (Fig. 8d).

Acknowledgments We thank Prof. I. Willner (Hebrew University of Jerusalem), Prof. R. Weinkauf (University of Dusseldorf), and Dr. S. Karthäuser (FZ Jülich) for stimulating discussions. The work of FR and RG was supported by the EC FET project MOLOC and the ARC grant of the French Community of Belgium NANOFORCE.

References

1. Lenoble C, Becker RS (1986) Photophysics, photochemistry, kinetics, and mechanism of the photochromism of 6'-nitroindolinospiropyran. J Phys Chem 90:62–65
2. Chibisov AK, Gorner H (1997) Photoprocesses in spiropyran-derived merocyanines. J Phys Chem A 101:4305–4312
3. Minkin VI (2004) Photo-, thermo-, solvato-, and electrochromic spiroheterocyclic compounds. Chem Rev 104:2751–2776
4. Minkin VI, Metelitsa AV, Dorogan IV, Lukyanov BS, Besugliy SO, Micheau J-C (2005) Spectroscopic and theoretical evidence for the elusive intermediate of the photoinitiated and thermal rearrangements of photochromic spiropyrans. J Phys Chem A 109:9605–9616
5. Buntinx G, Poizat O, Foley S, Sliwa M, Aloise S, Lokshin V, Samat A (2010) Sub-picosecond transient absorption spectroscopy of substituted photochromic spironaphthoxazine compounds. Dyes Pigm 89:305–312
6. Willner I (1997) Photoswitchable biomaterials: en route to optobioelectronic systems. Acc Chem Res 30:347–356
7. Berkovic G, Krongauz V, Weiss V (2000) Spiropyrans and spirooxazines for memories and switches. Chem Rev 100:1741–1754
8. Wen G, Yan J, Zhou Y, Zhang D, Mao L, Zhu D (2006) Photomodulation of the electrode potential of a photochromic spiropyran-modified Au electrode in the presence of Zn2+: a new molecular switch on the electronic transduction of the optical signals. Chem Commun 2006(28):3016–3018
9. Fukushima K, Vandenbos AJ, Fujiwara T (2007) Spiropyran dimer toward photo-switchable molecular machine. Chem Mater 19:644–646
10. Bardavid Y, Goykhman I, Nozaki D, Cuniberti G, Yitzchaik S (2011) Dipole assisted photogated switch in spiropyran grafted polyaniline nanowires. J Phys Chem C 115:3123–3128
11. Raymo FM, Alvarado RJ, Giordani S, Cejas MA (2003) Memory effects based on intermolecular photoinduced proton transfer. J Am Chem Soc 125:2361–2364
12. Tomizaki K-y, Mihara H (2007) Phosphate-mediated molecular memory driven by two different protein kinases as information input elements. J Am Chem Soc 129:8345–8352
13. Riskin M, Gutkin V, Felner I, Willner I (2008) Photochemical and electrochemical encoding of erasable magnetic patterns. Angew Chem Int Ed 47:4416–4420
14. Winkler JD, Bowen CM, Michelet V (1998) Photodynamic fluorescent metal ion sensors with parts per billion sensitivity. J Am Chem Soc 120:3237–3242
15. Ren J, Tian H (2007) Thermally stable merocyanine form of photochromic spiropyran with aluminium ion as a reversible photo-driven sensors in aqueous solution. Sensors 7:3166–3178
16. Scarmagnani S, Walsh Z, Slater C, Alhashimy N, Paull B, Macka M, Diamond D (2008) Polystyrene bead-based system for optical sensing using spiropyran photoswitches. J Mater Chem 18:5063–5071
17. Shiraishi Y, Adachi K, Itoh M, Hirai T (2009) Spiropyran as a selective, sensitive, and reproducible cyanide anion receptor. Org Lett 11:3482–3485
18. Zhu M-Q, Zhu L, Han JJ, Wu W, Hurst JK, Li ADQ (2006) Spiropyran-based photochromic polymer nanoparticles with optically switchable luminescence. J Am Chem Soc 128:4303–4309
19. Zhu L, Wu W, Zhu M-Q, Han JJ, Hurst JK, Li ADQ (2007) Reversibly photoswitchable dual-color fluorescent nanoparticles as new tools for live-cell imaging. J Am Chem Soc 129:3524–3526
20. de Leon L, Biewer MC (2000) Preparation of self-assembled monolayers with specific intermolecular interactions. Tetrahedron Lett 41:3527–3530
21. Wohl CJ, Kuciauskas D (2005) Excited-state dynamics of spiropyran-derived merocyanine isomers. J Phys Chem B 109:22186–22191
22. Holm A-K, Mohammed OF, Rini M, Mukhtar E, Nibbering ETJ, Fidder H (2005) Sequential merocyanine product isomerization following femtosecond UV excitation of a spiropyran. J Phys Chem A 109:8962–8968
23. Poisson L, Raffael KD, Soep B, Mestdagh J-M, Buntinx G (2006) Gas-phase dynamics of spiropyran and spirooxazine molecules. J Am Chem Soc 128:3169–3178
24. Stitzel S, Byrne R, Diamond D (2006) LED switching of spiropyran-doped polymer films. J Mater Sci 41:5841–5844
25. Kalisky Y, Orlowski TE, Williams DJ (1983) Dynamics of the spiropyran-merocyanine conversion in solution. J Phys Chem 87:5333–5338
26. Tamaki T, Sakuragi M, Ichimura K, Aoki K (1989) Laser photolysis studies of nitrospiropyrans intramolecularly linked with a triplet quenching or sensitizing side group. Chem Phys Lett 161:23–26

27. Helmut G (1998) Photochemical ring opening in nitrospiropyrans: triplet pathway and the role of singlet molecular oxygen. Chem Phys Lett 282:381–390
28. Emsting NP (1989) Transient optical absorption spectroscopy of the photochemical spiropyran-merocyanine conversion. Chem Phys Lett 159:526–531
29. Zhang JZ, Schwartz BJ, King JC, Harris CB (1992) Ultrafast studies of photochromic spiropyrans in solution. J Am Chem Soc 114:10921–10927
30. Chibisov AK, Gorner H (2001) Photochromism of spirobenzopyranindolines and spironaphthopyranindolines. Phys Chem Chem Phys 3:424–431
31. Sheng Y, Leszczynski J, Garcia AA, Rosario R, Gust D, Springer J (2004) Comprehensive theoretical study of the conversion reactions of spiropyrans: substituent and solvent effects. J Phys Chem B 108:16233–16243
32. Maurel F, Aubard J, Millie P, Dognon JP, Rajzmann M, Guglielmetti R, Samat A (2006) Quantum chemical study of the photocoloration reaction in the napthoxazine series. J Phys Chem A 110:4759–4771
33. Wojtyk JTC, Wasey A, Xiao N-N, Kazmaier PM, Hoz S, Yu C, Lemieux RP, Buncel E (2007) Elucidating the mechanisms of acidochromic spiropyran-merocyanine interconversion. J Phys Chem A 111:2511–2516
34. Hisayoshi S (1997) Molecular orbital calculations for acid induced ring opening reaction of spiropyran. Dyes Pigm 33:229–237
35. Buback J, Kullmann M, Langhojer F, Nuernberger P, Schmidt R, Wurthner F, Brixner T (2010) Ultrafast bidirectional photoswitching of a spiropyran. J Am Chem Soc 132:16510–16519
36. Krysanov SA, Alfimov MV (1984) Picosecond flash photolysis of photochromic spiropyrans. Laser Chem 4:129–138
37. Cottone G, Noto R, La Manna G (2004) Theoretical study of spiropyran-merocyanine thermal isomerization. Chem Phys Lett 388:218–222
38. Ernsting NP, Dick B, Arthen-Engeland Th (1990) The Primary photochemical reaction step of unsubstituted indolino-spiropyrans. Pure Appl Chem 62:1483–1488
39. Ipe BI, Mahima S, Thomas KG (2003) Light-induced modulation of self-assembly on spiropyran-capped gold nanoparticles: a potential system for the controlled release of amino acid derivatives. J Am Chem Soc 125:7174–7175
40. Riskin M, Willner I (2009) Coupled electrochemical/photochemical patterning and erasure of ag 0 nanoclusters on au surfaces. Langmuir 25:13900–13905
41. Piantek M, Schulze G, Koch M, Franke KJ, Leyssner F, Kruger A, Navio C, Miguel J, Bernien M, Wolf M, Kuch W, Tegeder P, Pascual JI (2009) Reversing the thermal stability of a molecular switch on a gold surface: ring-opening reaction of nitrospiropyran. J Am Chem Soc 131:12729–12735
42. Kiebwetter R, Pustet N, Brandl F, Mannschreck A (1999) 1′, 3′, 3′-Trimethyl-6-nitrospiro[2H-1-benzopyran-2,2′-indoline]: its thermal enantiomerization and the equilibration with its merocyanine. Tetrahedron Asymmetry 10:4677–4687
43. Frisch MJ, Trucks GW, Schlegel HB, Scuseria GE, Robb MA, Cheeseman JR, Scalmani G, Barone V, Mennucci B, Petersson GA, Nakatsuji H, Caricato M, Li HPHX, Izmaylov AF, Bloino J, Zheng G, Sonnenberg JL, Hada M, Ehara M, Toyota K, Fukuda R, Hasegawa J, Ishida M, Nakajima YT, Honda Y, Kitao O, Nakai H, Vreven T, Montgomery JA, JEP Jr, Ogliaro F, Bearpark M, Heyd JJ, Brothers E, Kudin KN, Staroverov VN, Kobayashi R, Normand J, Raghavachari K, A Rendell K, Burant JC, Iyengar SS, Tomasi J, Cossi M, Rega N, Millam JM, Klene M, Knox JE, Cross JB, Bakken V, Adamo C, J Jaramillo C, Gomperts R, Stratmann RE, Yazyev O, Austin AJ, Cammi R, Pomelli C, Ochterski JW, Martin RL, Morokuma K, Zakrzewski VG, Voth GA, Salvador P, Dannenberg JJ, Dapprich S, Daniels AD, Farkas JÖ, Foresman B, Ortiz JV, Cioslowski J, Fox DJ (2009) Gaussian 09 Revision A.1
44. Wang Y-G (2009) Examination of DFT and TDDFT methods II. J Phys Chem A 113:10873–10879
45. Yanai T, Tew DP, Handy NC (2004) A new hybrid exchange–correlation functional using the Coulomb-attenuating method (CAM-B3LYP). Chem Phys Lett 393:51–57
46. Zhao Y, Truhlar D (2008) The M06 suite of density functionals for main group thermochemistry, thermochemical kinetics, noncovalent interactions, excited states, and transition elements: two new functionals and systematic testing of four M06-class functionals and 12 other functionals. Theor Chem Account 120:215–241
47. Sumimoto M, Kawashima Y, Yokogawa D, Hori K, Fujimoto H (2012) Influences of dispersion and long-range corrections on molecular structures of three types of lithium phthalocyanine dimer. Int J Quantum Chem. doi:10.1002/qua.24072
48. Becke A (1993) Density-functional thermochemistry. III. The role of exact exchange. J Chem Phys 98:5648–5652
49. Mohan N, Vijayalakshmi KP, Koga N, Suresh CH (2010) Comparison of aromatic NH$\cdots\pi$, OH$\cdots\pi$, and CH$\cdots\pi$ interactions of alanine using MP2, CCSD, and DFT methods. J Comput Chem 31:2874–2882
50. Futami Y, Chin MLS, Kudoh S, Takayanagi M, Nakata M (2003) Conformations of nitro-substituted spiropyran and merocyanine studied by low-temperature matrix-isolation infrared spectroscopy and density-functional-theory calculation. Chem Phys Lett 370:460–468
51. Hobley J, Malatesta V, Millini R, Montanari L, Neil Parker WO (1999) Proton exchange and isomerisation reactions of photochromic and reverse photochromic spiro-pyrans and their merocyanine forms. Phys Chem Chem Phys 1:3259–3267
52. Buback J, Nuernberger P, Kullmann M, Langhojer F, Schmidt R, Wurthner F, Brixner T (2011) Ring-closure and isomerization capabilities of spiropyran-derived merocyanine isomers. J Phys Chem A 115:3924–3935
53. Meir R, Chen H, Lai W, Shaik S (2010) Oriented electric fields accelerate diels–alder reactions and control the endo/exo selectivity. ChemPhysChem 11:301–310
54. Singh UC, Kollman PA (1984) An approach to computing electrostatic charges for molecules. J Comput Chem 5:129–145
55. Reed AE, Weinstock RB, Weinhold F (1985) Natural population analysis. J Chem Phys 83:735–746
56. Shiraishi Y, Itoh M, Hirai T (2010) Thermal isomerization of spiropyran to merocyanine in aqueous media and its application to colorimetric temperature indication. Phys Chem Chem Phys 12:13737–13745
57. Campredon M, Giusti G, Guglielmetti R, Samat A, Gronchi G, Alberti A, Benaglia M (1993) Radical ions and germyloxyaminoxyls from nitrospiro[indoline-naphthopyrans]. A combined electrochemical and EPR study. J Chem Soc Perkin Trans 2:2089–2094
58. Preigh MJ, Stauffer MT, Lin F-T, Weber SG (1996) Anodic oxidation mechanism of a spiropyran. J Chem Soc Faraday Trans 92:3991–3996
59. Jukes RTF, Bozic B, Hartl F, Belser P, De Cola L (2006) Synthesis, photophysical, photochemical, and redox properties of nitrospiropyrans substituted with Ru or Os Tris(bipyridine) complexes. Inorg Chem 45:8326–8341
60. Wagner K, Byrne R, Zanoni M, Gambhir S, Dennany L, Breukers R, Higgins M, Wagner P, Diamond D, Wallace GG, Officer DL (2011) A multiswitchable poly(terthiophene) bearing a spiropyran functionality: understanding photo- and electrochemical control. J Am Chem Soc 133:5453–5462
61. Zhi JF, Baba R, Hashimoto K, Fujishima A (1995) A Multifunctional electro-optical molecular device. The photoelectrochemical behavior of spirobenzopyrans in dimethylformamide. Ber Bunsenges Phys Chem 99:32–39